Linear Quadratic Optimal Control Synthesis for a UAV

Fendy Santoso, Ming Liu and Gregory Egan

Department of Electrical & Computer Systems Engineering
Monash University, VIC 3800
Melbourne, Australia

Abstract

This paper depicts the application of linear quadratic optimal control to the longitudinal flight motion of an unmanned aerial vehicle (UAV) which has elevon control only. For a trimmed flight model obtained experimentally in previous study we develop in order a Linear Quadratic Regulators (LQR) controller followed by a Kalman filter based estimator for unmeasurable states. The LQR controller is then combined with the Kalman estimator using the separation principle to investigate the feasibility of altitude control. The simulation results show improvements compared with classical design counterparts in the sense that the combined approach offers more design flexibility and is able to tolerate the noisy environments. It shows reasonable altitude holding, taking off and landing performance. The schemes developed through this research will be incorporated in our existing autopilots.

Biography

Mr F. Santoso is a post-graduate student in the Department of Electrical & Computer Systems Engineering (fsan3@student.monash.edu.au, fendy_santoso@yahoo.co.uk).

Dr M. Liu is a Senior Lecturer and conducts research into control system optimisation techniques (ming.liu@eng.monash.edu.au).

Professor G.K. Egan is a Professor of Electrical & Computer Systems Engineering and Director of the Centre for Telecommunications and Information Engineering (greg.egan@eng.monash.edu.au).

Also published AIAC12, Melbourne, Australia, 16-22 March 2007.

Introduction

There has been an extremely rapid growth in interest in unmanned vehicles over the last several years. The advantages to be had from autonomous vehicles in a military environment are now well recognised with civil applications being in their infancy.

A general requirement for UAVs in particular is that they be inexpensive to operate. This cost can for civil applications be dominated by operator cost. Operators are generally not experts in aerodynamics and so require aircraft with robust and, where possible, automatically tuned control systems.

The UAVs of interest to us are small and fly at low Reynolds Numbers (250K) regimes which, amongst other challenges, mean turbulent flow and laminar separation across wing surfaces. Partially because of this, the aircraft dynamics are non-linear and at times uncertain. Aircraft of this size are also very susceptible to air turbulence.

This paper discusses a preliminary study of applying linear optimal control of altitude from pitch for an aircraft that has elevon control surfaces only. Our early identification work for the aircraft is published in [1] with extensions to this work in [2]. Relevant control theory may be found in [4], [5], [6], [7] and [8]. We have at our disposal a very large repository of flight logs for our aircraft obtained over several years. The logs contain a complete record of aircraft in-flight dynamics. It is intended to make this material available to other researchers for their control system studies.

Generating a comprehensive non-linear model for the aircraft is usually impractical. A more realistic approach is to develop a linearised model which is valid for a small dynamic range. Longitudinal and lateral models for conventional larger aircraft are well understood ([10][11][12][13]).

In this study, we consider time domain optimal control approaches using a LQR and Kalman filter estimator [9]. The combination of the two will lead to a Linear Quadratic Gaussian (LQG) controller that is more tolerant of uncertainty and noise in a real UAV flight environment. The design approach also offers several advantages compared with the classical PID controller. Positions of closed loop poles and overall performance can be adjusted by varying the values of weighting matrices accordingly. While control tool-boxes of the type found in MatLab make the composition process simple the offline algorithms are significantly more computationally intensive than the current simple PID based control loops computed online or in-flight where we have electrical and computational power limitations.

UAV Longitudinal Model

Most conventional aircraft have three primary control surfaces, namely, rudder, elevator and ailerons. Along with the throttle they are the four major input variables to control the flight of an aircraft. The aircraft used in this study (Fig. 1 and Table I.) is a flying wing and if unswept it is known as a "plank" because of its resemblance of course to a plank of wood. Most flying wings have only two control surfaces or elevons that combine the function of ailerons for roll control (and indirectly turn) and elevators for pitch control.

Planks are simple to construct and can be made to be very compact, rugged and crash tolerant. The flight characteristics of planks are benign, at least for human operators and they also exhibit predictable stall behaviour allowing them to descend quickly and safely. All of these characteristics were important in the design of P15035, its sister aircraft P16025 and the superficially similar Dragon Eye now widely deployed with the US Marines.

Flying wings, because they do not have a tail, rely on some reverse camber (upsweep in the trailing edge of the wing) to maintain a zero pitching moment and with that comes drag and less energy efficiency. To minimise the reverse camber we have to minimise the stability margin in the pitch axis. In this study, the stability margin has been made sufficiently high to allow human control. The controller described here will permit us to use airfoils with less camber and less drag both for computer assisted and autonomous flight.

Fig. 1 The P15035 Aircraft.
(reproduced with the permission of J. Bird
a member of the Aerobotics Group)

Pitch is controlled by the average deflection of the two elevons and roll (and indirectly yaw) by the difference, at least to a first order approximation. It is worth noting that for planks roll is normally controlled by deflecting the elevons equally in an attempt to control yaw and to again minimise unnecessary drag. It is feasible to control the elevons independently in a more optimum fashion rather than have them coupled in a relatively simple relationship. This will be developed

further in later research, but for now, we will concentrate on pitch-axis control where the elevons are driven in unison.

TABLE I
SPECIFICATIONS OF AIRCRAFT P15035

Span	150 cm	**Motor**	Electric
Chord	35 cm	**Duration**	40-60 minutes
Length	106 cm	**Speed**	33 to 150 Kph
Controls	Elevon	**Battery**	28×GP3300NiMh
Weight	2.9 to 4.6 Kg	**Autopilot**	MP2028

The longitudinal model and lateral directional model for the P15035 have been obtained using normal system identification techniques [11], [12] and [13] based on real flights, as distinct from simulation, and were initially reported in [1].

For trimmed flight with a constant engine thrust (and airspeed) the P15035's longitudinal discrete time transfer function from the elevon average deflection ∂ (degree) to the pitch angle θ (°) with a sampling frequency of 5 Hz is

$$\frac{\theta}{\delta} = \frac{-0.13065z^2(z+0.0091)}{(z-0.9115)(z-0.9785)(z^2+0.2267z+0.3763)} \quad . \quad (1)$$

Converted to s domain, it becomes:

$$\frac{\theta(s)}{\delta(s)} = \frac{-0.2954(s+6.693)(s^2+11.7s+91.49)}{(s+0.4633)(s+0.1087)(s^2+4.887s+83.12)} . \quad (2)$$

It is apparent that as all poles of (2) are located on the left hand side of the s plane so the open loop system is stable as we expect.

It has been established (e.g., see [3], [4], [5] and [15]) that the typical longitudinal dynamics of a traditional aircraft (elevator to pitch) with a constant engine thrust can be expressed as

$$\frac{\theta(s)}{\delta(s)} = \frac{k_\theta(s+1/T_{\theta_1})(s+1/T_{\theta_2})}{(s^2+2\zeta_p\omega_p s+\omega_p^2)(s^2+2\zeta_s\omega_s s+\omega_s^2)}, \quad (3)$$

where δ is now the elevator angle (instead of the elevon average in (2)). For aircraft, the factor $\Delta s_p = s^2+2\zeta_p\omega_p s+\omega_p^2$ in the characteristic equation of (3) is termed the phugoid mode, and the second one $\Delta s_s = s^2+2\zeta_s\omega_s s+\omega_s^2$ is the short period mode. Typically, the phugoid mode is overdamped with a relatively large time constant and the short period mode represents under-damped oscillation. The overall pitch step response is a combination of a slow exponential function and a quickly decaying high frequency oscillation.

Comparing (2) with (3), it can be seen that the longitudinal model (2) has pitch characteristics which are similar to those of conventional aircraft. Its phugoid model is

$$\Delta s_p = (s+0.4633)(s+0.1087) \cdot \quad (4)$$

This is overdamped with a dominant large time constant of T=10s. Its short period model is given by:

$$\Delta s_s = s^2+4.887s+83.12 . \quad (5)$$

Here the damping ratio is 0.268 and the natural frequency 9.12 rad/s. The settling time is small being in the order of 1s. The impulse response for both modes is plotted in Fig. 2.

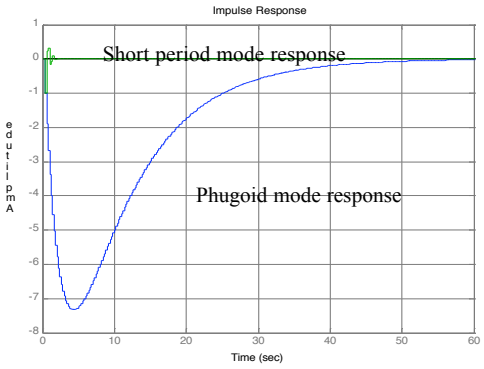

Fig. 2 Impulse pitch amplitude responses in degrees for phugoid and short period modes of UAV P15035.

Optimal Flight Controller Design

Having confirmed that the longitudinal response is of the general form expected, we now determine the pitch-to-altitude transfer function in z domain with a sampling frequency of 5 Hz as

$$\frac{h(z)}{\theta(z)} = \frac{0.05456z}{z-0.9969} . \quad (6)$$

Converting (6) to s domain and cascading it with (2), we obtain the following transfer function

$$\frac{h}{\delta} = \frac{-0.011659(s^2+11.88s+42.46)(s^2+9.723s+99.83)}{(s+0.4633)(s+0.1087)(s+0.01552)(s^2+4.887s+83.12)} \quad (7)$$

where h is the altitude of the aircraft in metres.

State Equations

Converting (7) into its state space counterparts, we have the following state space description

$$\begin{aligned} \dot{x} &= Ax + Bu \\ y &= Cx + Du \end{aligned} , \quad (8)$$

in which,

$$A = \begin{bmatrix} -5.4740 & -86.0500 & -49.120 & -4.9270 & -0.0650 \\ 1 & 0 & 0 & 0 & 0 \\ 0 & 1 & 0 & 0 & 0 \\ 0 & 0 & 1 & 0 & 0 \\ 0 & 0 & 0 & 1 & 0 \end{bmatrix}$$

$$B = \begin{bmatrix} 1 & 0 & 0 & 0 & 0 \end{bmatrix}^T$$

$$C = \begin{bmatrix} -0.0117 & -0.2519 & -3.0060 & -18.640 & -49.4200 \end{bmatrix}$$

$$D = [0].$$

For an LQR controller, the system to be controlled has to be both controllable and observable for all states as is the case for (8).

LQR Controller

Under the assumption that all state variables are available for feedback, in what follows, we consider the LQR design. For a given quadratic cost function

$$J = \int_0^\infty (x^T Qx + u^T Ru)dt, \qquad (9)$$

in which Q, $R \geq 0$ are real state and input weighting matrices respectively. The objective is to determine an optimal state feedback control law

$$u = -kx, \qquad (10)$$

which can drive all state variables rapidly to their equilibrium point. By considering the following Ricatti Equation

$$A^T P + PA - PBR^{-1}B^T P + Q = 0. \qquad (11)$$

we can determine the solution for P and the optimal gain k is now

$$k = R^{-1}B^T P. \qquad (12)$$

The closed loop poles are moved to provide ideal performance.

Performance Test

Fig. 3 shows the unit step responses for different weighting matrices Q and R. The overshoot is not significant as the overall closed loop system is still dominated by phugoid poles which are located on the real axis.

Fig. 4 displays how incrementing Q affects the location of the closed loop poles whilst R is kept constant. As the values of Q increase form 10I to 100I with a step size of 10, the locations of 2 conjugate closed loop poles gradually shift to the left and the position of the other 3 dominate poles remain relatively unchanged. The damping factors of 2 poles on the far left increase gradually from 0.32 to 0.611 as Q is increased from 10I to 100I. At the same time the damping factors of 2 poles near the imaginary axis decrease slightly from 0.687 to 0.632. Meanwhile, the damping factor of fifth pole on the real axis remains unchanged and determines the large time constant of the exponential component of the response. Generally speaking, there are slight increases for the undamped natural frequency as Q increases in the range 0.36 to 0.46 rad/s.

It is easy to understand that a larger state error-weighting matrix Q leads to greater control action and therefore larger feedback gain K (Fig. 5). As a consequence, an input gain scaling N is used for each value of Q (Fig. 6). It is apparent that the larger the value of weighting matrices Q the smaller the value of its corresponding gains adjustments. Starting from Q = 10I, the value of N decrease gradually from almost -0.06 to about 0.2 when Q is set to be 100I.

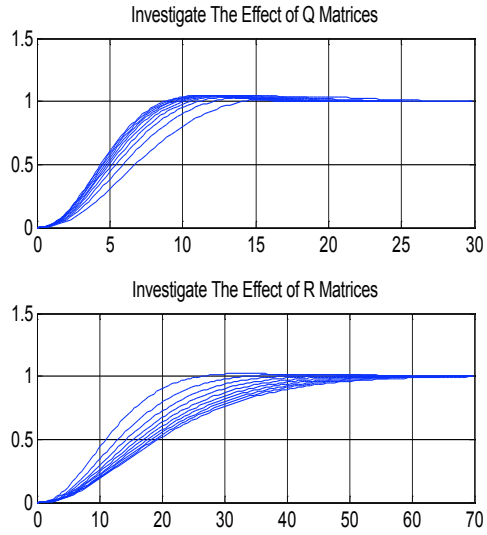

Fig. 3 Step responses of altitude for varying Q and R in which the top plot shows for fixed $R = I$ the larger Q the quicker response and the bottom plot shows for fixed $Q = I$ the larger R the slower response.

If R is varied and Q remains constant, the locations of closed loop poles remain relatively unchanged, as shown in Fig. 7. There are slight decreases in the un-damped natural frequency as R increases and a slight shift to the right of the closed loop poles. Larger Q and smaller R values will result in an energy saving through a reduced control action. Because k is smaller there is a slower closed loop response and a longer time to reach a steady state value. Fig. 9 shows the gain scaling factors as the control weighting matrix increases.

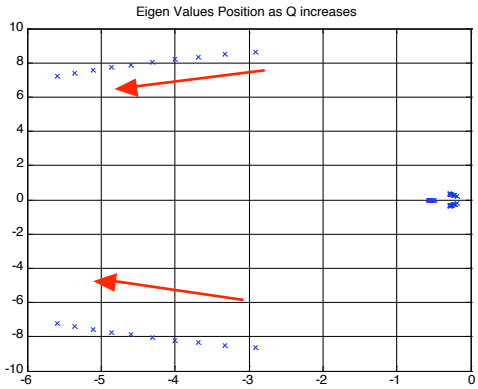

Fig. 4 Effects of Q vis closed loop poles' locations

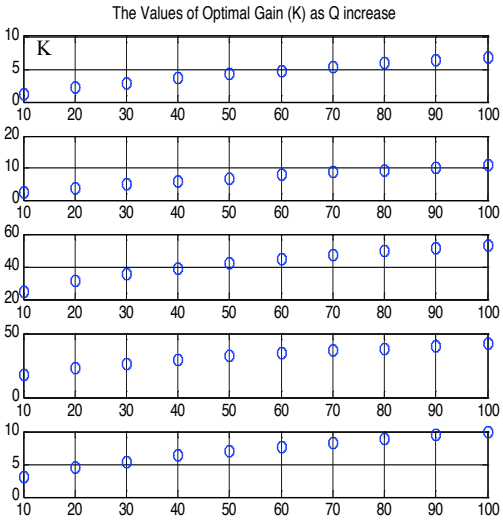

Fig. 5 Value of optimal gain for each state feedback channel affected by Q

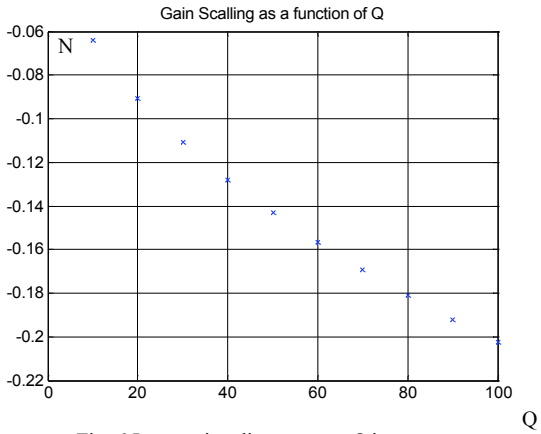

Fig. 6 Input gain adjustment as Q increases

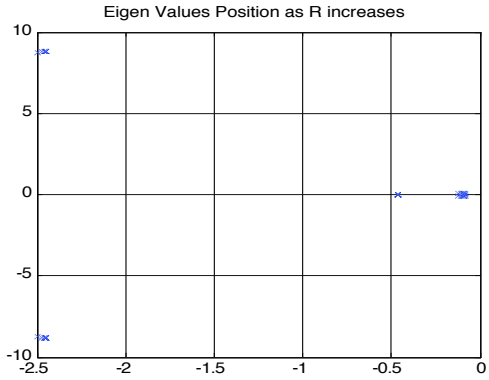

Fig. 7 Effects of R vs closed loop poles' locations

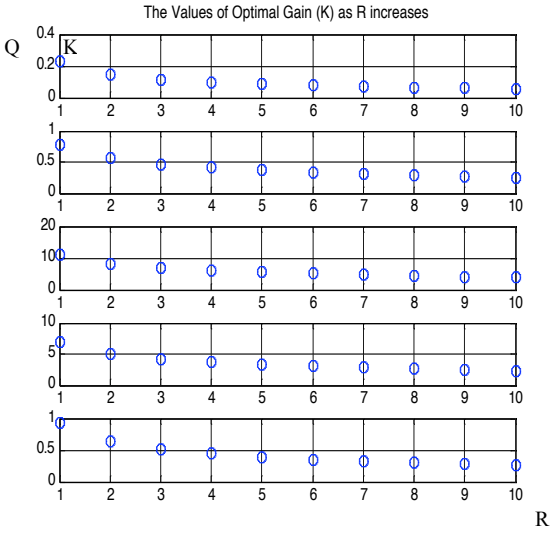

Fig. 8 Value of optimal gain for each state feedback channel affected by R

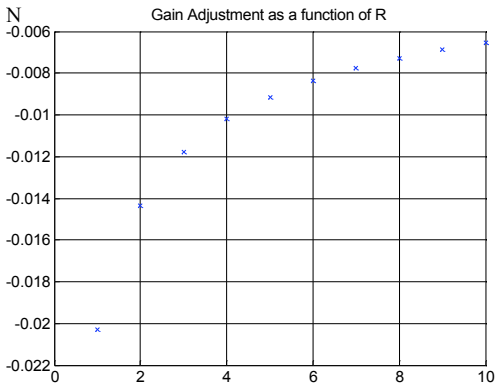

Fig. 9 Input gain adjustments as R increases

Kalman Filter

In last section, we designed the LQR controller using state feedback under the assumption that all state variables are measurable. However, in practice, this assumption is unlikely to be true. In our application of autopilot design only two state variables altitude and airspeed may be available. In this section we consider the Kalman filter for state estimation. Given the following state and output equations

$$\begin{aligned} \dot{x} &= Ax + Bu + Fw \\ y &= Cx + v \end{aligned}, \quad (13)$$

where w and v are process and sensor noise respectively, we introduce a state estimator (14)

$$\begin{aligned} \dot{\hat{x}} &= A\hat{x} + Bu + L(y - \hat{y}) \\ \hat{y} &= C\hat{x} \end{aligned}, \quad (14)$$

where $\hat{x}$ is an estimate of x. The overall state equations may be obtained from (13) and (14) as

$$\begin{bmatrix} \dot{x} \\ \dot{\hat{x}} \end{bmatrix} = \begin{bmatrix} A & 0 \\ LC & A - LC \end{bmatrix} \begin{bmatrix} x \\ \hat{x} \end{bmatrix} + \begin{bmatrix} B & F & 0 \\ B & 0 & L \end{bmatrix} \begin{bmatrix} u \\ w \\ v \end{bmatrix}. \quad (15)$$

Let S_w and S_v be the spectral densities of zero mean white noise w and v respectively, the optimal estimation gain L vector is given by

$$L = PC^T S_v^{-1}, \quad (16)$$

in which, P is the solution of the following equation:

$$PA^T + AP + FS_wF^T - PC^T S_v^{-1} CP = 0. \quad (17)$$

The Kalman filter altitude estimation estimation compared with its real value for S_w, S_v = 1.0 are shown in Fig. 10. Its gain L is given by

$$L = [0.0016 \;\; 0.0024 \;\; -0.0032 \;\; -0.0132 \;\; -0.0188]^T. \quad (18)$$

For $S_w = 100\,N^2m^2/Hz$ and $S_v = 1\deg^2/Hz$, which correspond to a process noise of 1w and a sensor noise of 0.01w. The optimal gain is

$$L = [0.2178 \;\; 0.0177 \;\; -0.0769 \;\; -0.0721 \;\; -0.0315]^T. \quad (19)$$

Linear Quadratic Gaussian Design

Using a Kalman filter we were able to obtain the estimates of unmeasurable flight states. By combining the Kalman filter and LQR control, the estimated state variables can be used to replace the unmeasurable state x in (10) to give

$$u = -k\hat{x} + r, \quad (20)$$

where r is the reference input signal and $\hat{x}$ is the estimated state obtained using the Kalman filter. The design objective is to minimize a quadratic cost function given by the limit

$$J_{LQG} = \lim_{T\to\infty} \int_0^T \left\{ [x' \;\; u'] W \begin{bmatrix} x \\ u \end{bmatrix} \right\} dt. \quad (21)$$

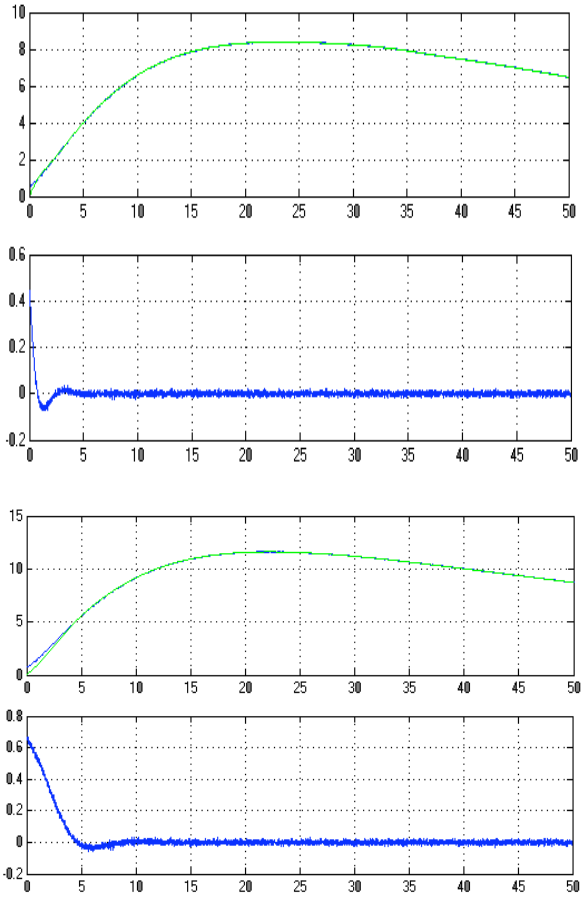

Fig. 10 Real altitude, its estimate and estimation error for Sw=1 and Sv=1 (top two plots) and Sw=100 and Sv=1 (bottom two plots)

By combining the Kalman filter and LQR equations, we obtain the following augmented matrix:

$$\begin{bmatrix} \dot{x} \\ \dot{\hat{x}} \end{bmatrix} = \begin{bmatrix} A & -Bk \\ LC & (A - LC - Bk) \end{bmatrix} \begin{bmatrix} x \\ \hat{x} \end{bmatrix} + \begin{bmatrix} B & F & 0 \\ B & 0 & L \end{bmatrix} \begin{bmatrix} r \\ w \\ v \end{bmatrix}, \quad (22)$$

where L, given by (16), is the Kalman filter feedback gain.

The LQG design leads to the optimal gain

$$K = [1.2252 \;\; 2.4575 \;\; 24.8761 \;\; 17.3437 \;\; 3.0980]. \quad (23)$$

The resulting closed loop eigenvalues, their damping ratios and undamped natural frequencies are given in Table II.

TABLE II
CLOSED LOOP CHARACTERISTICS OF LQG CONTROL

No	Eigenvalues	Damping	Frequency
1	-2.91 + 8.64i	0.32	9.12
2	-2.91 - 8.64i	0.32	9.12
3	-0.486	1.00	0.486
4	-0.192 + 0.203i	0.687	0.280
5	-0.192 – 0.203i	0.687	0.280

The Kalman filter optimal gain is now given by

$$L = [0.2178\ 0.0177\ -0.0769\ -0.0721\ -0.0315]^T \quad (24)$$

and its closed loop characteristics are given in Table III.

TABLE III
CLOSED LOOP CHARACTERISTICS OF KALMAN FILTER

No	Eigenvalues	Damping	Frequency
1	-2.44 + 8.78i	0.268	9.12
2	-2.44 - 8.78i	0.268	9.12
3	-0.958 + 1.55i	0.526	1.82
4	-0.958 - 1.55i	0.526	1.82
5	-1.79	1.00	1.79

The closed loop performance of altitude control, including takeoff, altitude hold and landing using the LQG controller is shown in Fig. 11. In the simulation, the altitude command is a step function of 100m, hold at 100m and step back to 0m at t=25s. Noise was included during the simulation to determine how effectively noise is rejected. The results show acceptable performance with zero steady state error and smooth transition response. It has been assumed that airspeed remains constant in the airspeed from throttle loop.

Conclusion

LQR, Kalman filter and LQG linear optimal approaches were applied to control of the altitude from pitch control loop of an elevon controlled flying wing. It was shown that the LQG controller formed from a combination of LQR controller and Kalman filter provides substantial flexibility through the choice of appropriate weighting matrix values. This flexibility includes tuning the controller for reduced control servo energy consumption albeit with longer settling times. Such flexibility is important as control servos are the greatest consumers of electrical energy even on P15035 which has only two servos; more conventional aircraft have upwards of six servos. We can choose to switch between fast response, high energy and slower response but lower energy consumption in-flight.

We are currently exploring how we may best implement this research in our current autopilots [17].

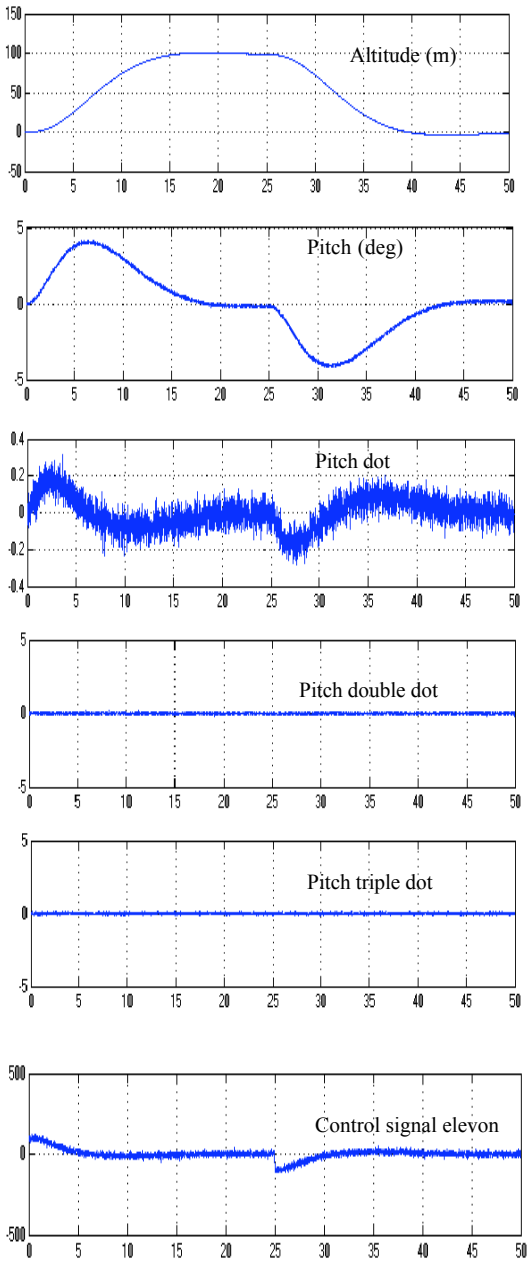

Fig. 11 LQR controller performance for take off, altitude holding and landing in which noise intensities are Sw =100 and Sv = 1

Acknowledgement

The authors wish to thank Mr. Raymond Cooper, the Chief Test Pilot in our group, for his coordination of all test flights and the construction of the P15035 aircraft. We also wish to thank the members of the Aerobotics Research Group at Monash University [16].

References

1. Liu, Ming, Egan, Gregory and Ge, Yunjian, Identification of Attitude Flight Dynamics for an Unconventional UAV" *Proc. of IEEE/RSJ International Conference on Intelligent Robots and Systems,* Oct. 9-15, Beijing, China, 2006.
2. Santoso, Fendy, *Robot Aircraft Dynamics Model Identification and Autopilot Designs*, Masters Thesis, Monash University, 2006.
3. Bryson, Arthur J.R., *Control of Spacecraft and Aircraft,* Princeton University Press, NJ, 1994.
4. Al-Shamary, Naim, *Robust and Gain Scheduled Flight Control Systems*, Masters Thesis, Monash University, 2001
5. Stevens, L Brian, Lewis, Frank, *Aircraft Control and Simulation*, John Wiley & Sons, Inc, 2nd edition, 2003
6. Ogata Katsuhiko, *Modern Control Engineering*, Prentice Hall, 2002
7. Franklin Gene F. et al, *Digital Control of Dynamic Systems*, Addison-Wesley Pub. Co., c1990
8. Franklin, Gene, et al, *Feedback Control of Dynamics Systems*, Pearson Prentice Hall, NJ, 2006
9. Kulcsar, Balazs, *LQG/LTR Controller Design for an Aircraft Model*, Periodica Polytechhica Ser, Vol. 28, No. 1-2, PP 131-142, 2000
10. Goodwin, Graham C and Payne, Robert L, *Dynamic system identification: Experiment design and data analysis*, Academic Press, INC London, LTD., 1977
11. Sage, Andrew P. and Melsa, James L., *System Identification*, Academic Press, INC, London, LTD., 1971.
12. Eykhoff, Pieter, *System Identification: Parameter and State Estimation*, John Wiley & Sons, 1974
13. Mehra, Raman K. and Lainiotis, Dimitri G., *System Identification Advances and Case Studies*, Academic Press, INC. (London) LTD, 1976
14. Welch, Greg, Bishop, Gary, *An Introduction to Kalman Filter*, University of North California at Chapel Hill, 2001
15. Pratt., Roger, *Flight control systems: practical issues in design and implementation*, The Institution of Electrical Engineers, UK, 2000
16. *Monash Aerobotics*, [online], Available: http://www.ctie.monash.edu.au/hargrave/aerobotics.html, 2002, (Accessed February 2006).
17. Micropilot, http://www.micropilot.com (Accessed January 2007).